MOLECULAR IMAGING AND BIOLOGY

Published Online: 1 December 2009

Mol Imaging Biol (2010) 12:250–258
DOI: 10.1007/s11307-009-0277-1

RESEARCH ARTICLE

Feasibility of Template-Guided Attenuation Correction in Cat Brain PET Imaging

Jin Su Kim,[1,2] Jae Sung Lee,[1,3] Min-Hyun Park,[4,5] Kyeong Min Kim,[2] Seung-Ha Oh,[4] Gi Jeong Cheon,[2] In Chan Song,[6] Dae Hyuk Moon,[7] June-Key Chung,[1,3] Dong Soo Lee[1]

[1]*Department of Nuclear Medicine and Interdisciplinary Program in Radiation Applied Life Science, Seoul National University College of Medicine, Seoul, Korea*
[2]*Molecular Imaging Research Center, Korea Institute of Radiological and Medical Sciences, Seoul, Korea*
[3]*Department of Biomedical Sciences, Seoul National University College of Medicine, Seoul, Korea*
[4]*Department of Otolaryngology and Research Center for Sensory Organs, Medical Research Center, Seoul National University College of Medicine, Seoul, Korea*
[5]*Department of Otolaryngology, Seoul Metropolitan Government Boramae Medical Center, Seoul, Korea*
[6]*Department of Radiology, Seoul National University Hospital, Seoul, Korea*
[7]*Department of Nuclear Medicine, Asan Medical Center, University of Ulsan College of Medicine, Seoul, Korea*

Abstract

Purpose: Attenuation correction (AC) is important in quantitative positron emission tomography (PET) imaging of medium-sized animals such as the cat. However, additional time for transmission (TX) scanning and tracer uptake is required in PET studies with animal-dedicated PET scanners because post-injection TX scanning is not available in these systems. The aim of this study was to validate a template-guided AC (TGAC) method that does not require TX PET data for AC in cat 2-deoxy-2-[F-^{18}fluoro-D-glucose (FDG) brain PET imaging.

Methods: PET scans were acquired using a microPET Focus 120 scanner. TX data were obtained using a ^{68}Ge point source before the injection of FDG. To generate the attention map (μ-map) template for the TGAC, a target image of emission (EM) PET was selected, and spatial normalization parameters of individual EM data onto the target were reapplied to the corresponding μ-maps. The inverse transformations of the μ-map template into the individual spaces were performed, and the transformed template was forward projected to generate the AC factor. The TGAC method was compared with measured AC (MAC) and calculated AC (CAC) methods using region of interest (ROI) and SPM analyses.

Results: The ROI analysis showed that the activity of the TGAC EM PET images strongly correlated with those of the MAC data ($y = 0.98x + 0.01$, R^2=0.96). In addition, no significant difference was observed in the SPM analysis. By contrast, the CAC showed a significantly higher uptake in the deep gray regions compared to the MAC (corrected P<0.05). The ROI correlation with MAC was worse than with the TGAC (R^2=0.84). In SPM analysis for the voxel-wise group comparisons between before and after the induction of deafness, only the TGAC showed equivalent results with the MAC.

Conclusions: The TGAC was reliable in cat FDG brain PET studies in terms of compatibility with the MAC method. The TGAC might be a useful option for increasing study throughput and decreasing the probability of subject movement. In addition, it might reduce the possible biological effects of long-term anesthesia on the cat brain in investigations using animal-dedicated PET scanners.

Key words: Attenuation correction, Animal PET, Spatial normalization, Cat, Brain

Correspondence to: Jae Sung Lee; *e-mail:* jaes@snu.ac.kr

Introduction

Imaging of the brain with positron emission tomography (PET) in animals is an important technology used by translational biomedical investigators for many purposes, i.e., the development of new CNS drugs and neuronal prostheses [1, 2] as well as investigations of the biochemical and molecular basis of normal functioning and pathology of the brain. Although non-human primates are ideal animal models, given their close genetic and anatomical similarities to humans, they are not widely available due to the ethical issues mainly associated with their evolutionary proximity to human beings and the high cost of conducting such research [3]. Recent advances in small animal-dedicated PET scanners with high resolution and sensitivity have facilitated neuroimaging studies on rodents, a much easier research model to use compared to non-human primates. However, the assessment of regional activity with anatomical detail is limited due to the small size of their brain.

Previous studies conducted by our group and other investigators have shown that the small-animal-dedicated PET scanners are also suitable for brain imaging studies of medium-sized animals such as cats and rabbits [4–7]. PET imaging studies on these animals have several advantages as models for sensory deprivation and the efficacy of neuronal prostheses since the surgical procedure is much easier than on rodents, and there is accumulated knowledge on the sensory systems of these animals.

Little attention has been focused on corrections of photon attenuation and Compton scattering in rodent PET imaging. However, there is a report that the physical artifact correction is important even in small animals such as mice [8]. These physical artifacts should be seriously considered in the brain PET scans of medium-sized animals because of their larger head size and thicker skull. Although the quantitative accuracy could benefit from correcting these physical factors, using the transmission (TX) PET scan data acquired with external radiation sources, these corrections are technically challenging procedures in the brain PET scans of medium-sized animals. Since post-injection TX PET scans [9] or the X-ray CT-based attenuation correction [10–12] are not available in most commercial small-animal PET scanners (i.e., microPET series of Siemens), additional time for performing TX scanning and waiting for the radiotracer uptake is required for the attenuation and scatter corrections. Based on our experience with TX scanning of the cat brain using a ^{68}Ge point source, at least 40 min was needed to obtain TX data with sufficient count rates to allow these corrections to be made [4, 6] even though the data were acquired under singles-mode conditions, which is more efficient than the conventional coincidence-mode acquisition [8, 10]. Although attenuation correction (AC) with singles-mode TX data acquired for less than 10 min using a ^{57}Co point source was reliable for rodent phantoms [13], longer scan time would be required for imaging cat brain because of the higher amount of photon attenuation.

In addition, the software currently used for segmented attenuation correction [14–16] in the commercial system used to reduce TX scanning times does not provide anatomically correct μ-maps for cat brain PET. Especially, this method is not reliable for noisy images [13]. These time demands require that the cats must be placed on an imaging bed while anesthetized for more than 60–90 min during the PET imaging studies, thus, reducing study throughput and increasing the probability of subject movement, e.g., due to an animal awakening during the study, in addition to the possible biological effects of long-term anesthesia.

Therefore, investigation of the feasibility of the AC method that does not require TX scanning, by estimating the spatial distribution of attenuation coefficients, only using the emission (EM) PET data (TX-less AC methods), is needed. In this study, we evaluated a template-guided AC (TGAC) method that was originally introduced for human brain PET data [17, 18] for cat 2-deoxy-2-[F-^{18}]fluoro-D-glucose (FDG) brain PET. In addition, this method was compared with the calculated AC (CAC) method [19, 20] with regard to compatibility with the measured AC (MAC), which is used as the gold standard.

Materials and Methods

PET Data

For the comparison of AC methodologies, 16 FDG brain PET data sets acquired from eight cats (weight=2.5±0.2 kg) on two occasions, which were used for optimization of the voxel-based statistical analysis of cat brain PET [4], were retrospectively analyzed. Briefly, the data were acquired before and 4 months after the induction of deafness using a microPET Focus 120 scanner [21]. The study was approved by the institutional animal care and use committee of Seoul National University. After achieving anesthesia, 40 min of TX data was acquired using a ^{68}Ge point source in singles mode. Thirty minutes after the intravenous injection of 1 mCi/kg FDG, 30 min of EM data was acquired. The EM data were reconstructed by 3DRP [22] and the TX data were reconstructed by OSEM (subset=16, iteration=4) algorithms.

All TX and blank data were corrected for the intrinsic ^{176}Lu activity [8, 23].

Attenuation coefficient was calibrated for the compensation of photon scatter by scaling the mean values of the attenuation coefficient map (attenuation map or μ-map) in the brain region, up to the theoretical attenuation coefficient of 511 keV gamma rays in soft tissue (0.095 cm^{-1}) [10]. The calibrated μ-map was then converted into the attenuation correction factor (ACF) by a forward projection, which was used for the MAC. The MAC data were used as the gold standard in the current study, since there was no contamination on the μ-map from the activity of the injected compounds. Scatter correction (SC) was performed for both the EM and TX data using a single scatter simulation scatter correction algorithm [24].

TX-less AC Methods

TGAC This method requires the standard templates of EM activity distribution and the μ-map (EM and μ-map templates), which are generally the averages of multiple data sets spatially normalized in

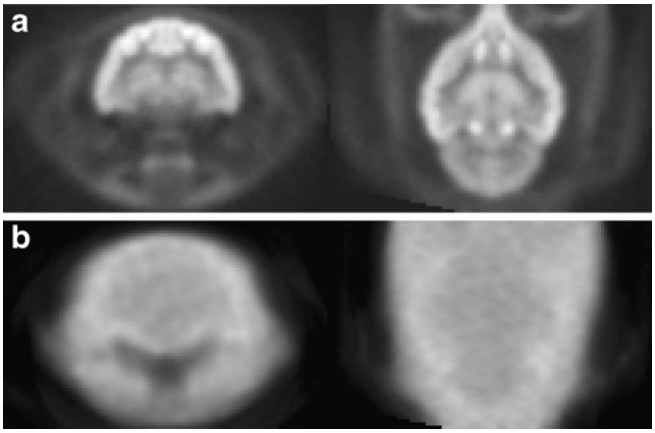

Fig. 1. Coronal and transverse slices of emission (**a**) and μ-map (**b**) templates of the cat brain PET.

the standard image coordinates. First, we generated the EM template, which was not corrected for attenuation and scatter using procedures established in our previous study [4]; the uncorrected EM image, with the best quality and symmetric shape, was selected as targets and smoothed using an isotropic Gaussian kernel with a full width at half maximum of 2 mm.

The individual EM images were spatially normalized onto the target image using only the affine transformation and then averaged. Although the CAC EM images were used in the human application of the TGAC [18], we used uncorrected EM data for template generation; this was because the CAC showed limited quantitative accuracy in the cat brain PET data from our preliminary assessments [7]. To generate a μ-map template for the TGAC, spatial normalization parameters for the individual EM data points onto the target brain were reapplied to the corresponding μ-map. The spatially normalized μ-maps from all 16 studies were averaged to obtain the μ-map template.

Individual EM images were then spatially normalized onto the EM template using affine and non-linear transformations using basis function [25, 26], and inverse transformations of the μ-map template into the individual space using the transformation parameters acquired from the EM images were performed to obtain the template-guided μ-map for individual data sets. The template-guided μ-maps were then forward projected from the image space to the sinogram space to generate the ACFs. The span number and ring difference of the generated ACFs were the same as the EM sinograms (span number=3, ring difference=47).

CAC CAC routine implemented in the data analysis software (ASIpro version 5.2.2.8) was used. A uniform μ-map was obtained by assigning the known linear attenuation coefficient of 511 keV gamma rays for soft tissue (0.095 cm^{-1}) to the whole head region of the cat and forward projected to generate the ACF. The EM sinograms were then corrected for attenuation and scatter using the ACF that was derived from either the template-guided or uniform μ-map data sets.

Statistical Analysis

The compatibility of the TX-less AC methods with the MAC method was evaluated by comparing the μ-maps and corrected EM images (EM_{AC}) obtained using the above described methods. Both the region of interest (ROI) and voxel-based analyses were performed. MRIcron and SPM5 software [25, 26] were used for these analyses.

ROI Analysis Twenty eight ROIs (frontal, parietal, and occipital lobes; precentral, postcentral, superior temporal, middle temporal, inferior temporal, and cingulate gyri; thalamus; caudate head; inferior colliculus; and superior colliculus in both hemispheres) were used for the ROI analysis [4]. The ROIs were drawn on the EM_{AC} by MAC using MRIcron software. The regional mean count of the ROIs were calculated and normalized to the mean count of the whole brain. Linear regression analyses between the TX-less AC methods and MAC method were performed. Correlation coefficients between methods were compared using Fisher's r to Z transformation.

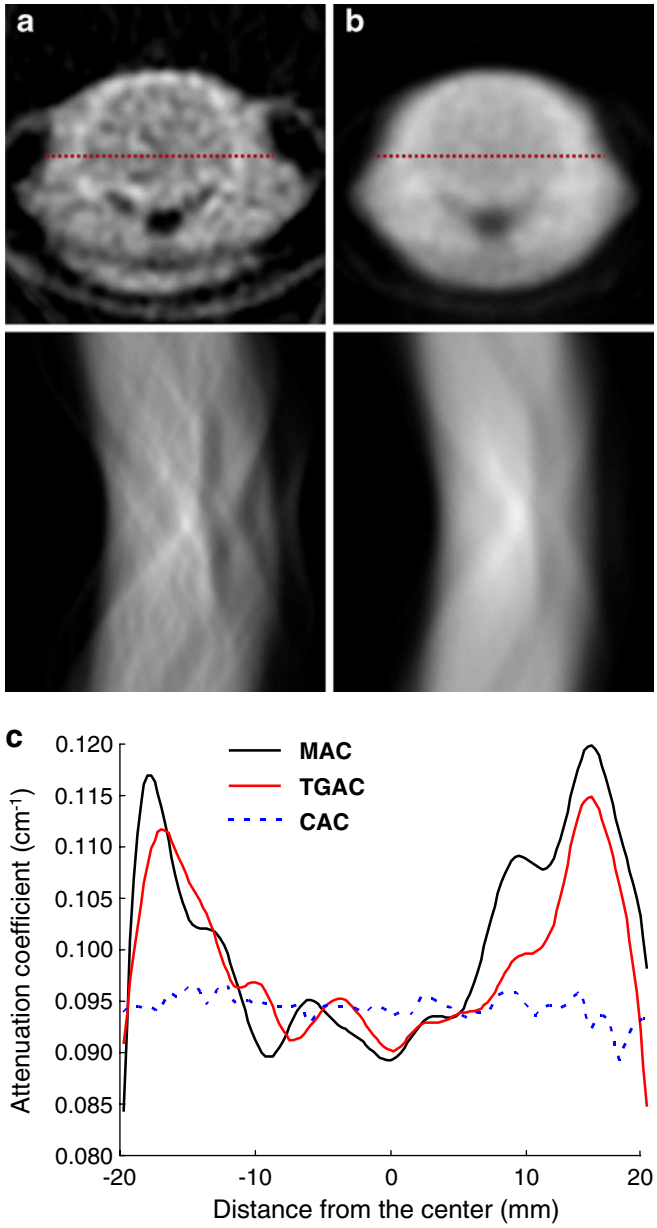

Fig. 2. The μ-maps and attenuation correction factors obtained using MAC (**a**) and TGAC (**b**) methods. **c** Counts profile across the center of μ-maps (*red dotted line*).

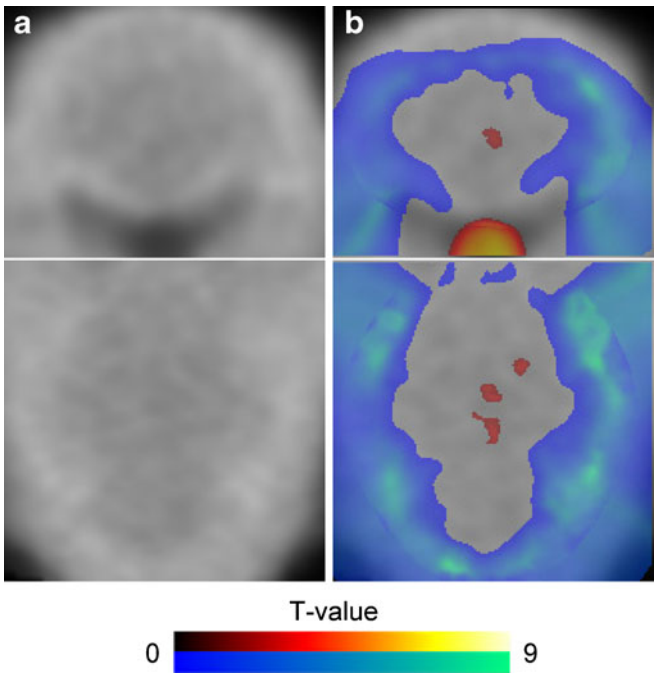

Fig. 3. The regions showing higher (*red color*) and lower (*blue color*) attenuation coefficients in the TGAC (**a**) and the CAC (**b**) compared to the MAC.

SPM Analysis Voxel-wise comparisons were performed on μ-maps and EM_{AC}. Transformation parameters obtained in the spatial normalization of the individual EM_{AC} by MAC onto the EM_{AC} template that was generated in our previous study [4] were identically applied to the EM_{AC} by the TX-less AC methods to remove the confounding effects of the different geometrical transformations. These parameters were also used for the spatial normalization of the μ-maps.

The voxel size of the spatially normalized images was set to $0.3 \times 0.3 \times 0.3$ mm. Both the μ-map and EM_{AC} were then smoothed with a 3-mm isotropic Gaussian kernel. Count normalization was not performed for the μ-maps to assess the absolute differences between μ-maps. The pixel values of the EM_{AC} were count normalized using the proportional scaling method with SPM software. Finally, voxel-wise paired t tests were performed to identify the regions with different attenuation coefficients or radioactivity between the TX-less AC and MAC methods.

For each AC method, comparisons between the data sets acquired before and 4 months after the induction of deafness was also performed to explore whether the TX-less AC method had compatible SPM results with the MAC method.

Further Validation

The cats underwent PET scans again 9 months after the induction of deafness, and the PET data were processed in the same way. Voxel-wise comparisons between the baseline and 9-month EM_{AC} images were performed to evaluate the usefulness of the TX-less AC method for longitudinal follow-up studies. Comparison between each individual deaf data set and all eight baseline data sets was also performed.

Results

Coronal and transverse slices of the EM and μ-map templates are shown in Fig. 1. The templates had the average features of the shape and intensity from the individual data. The air cavities and soft tissues were well

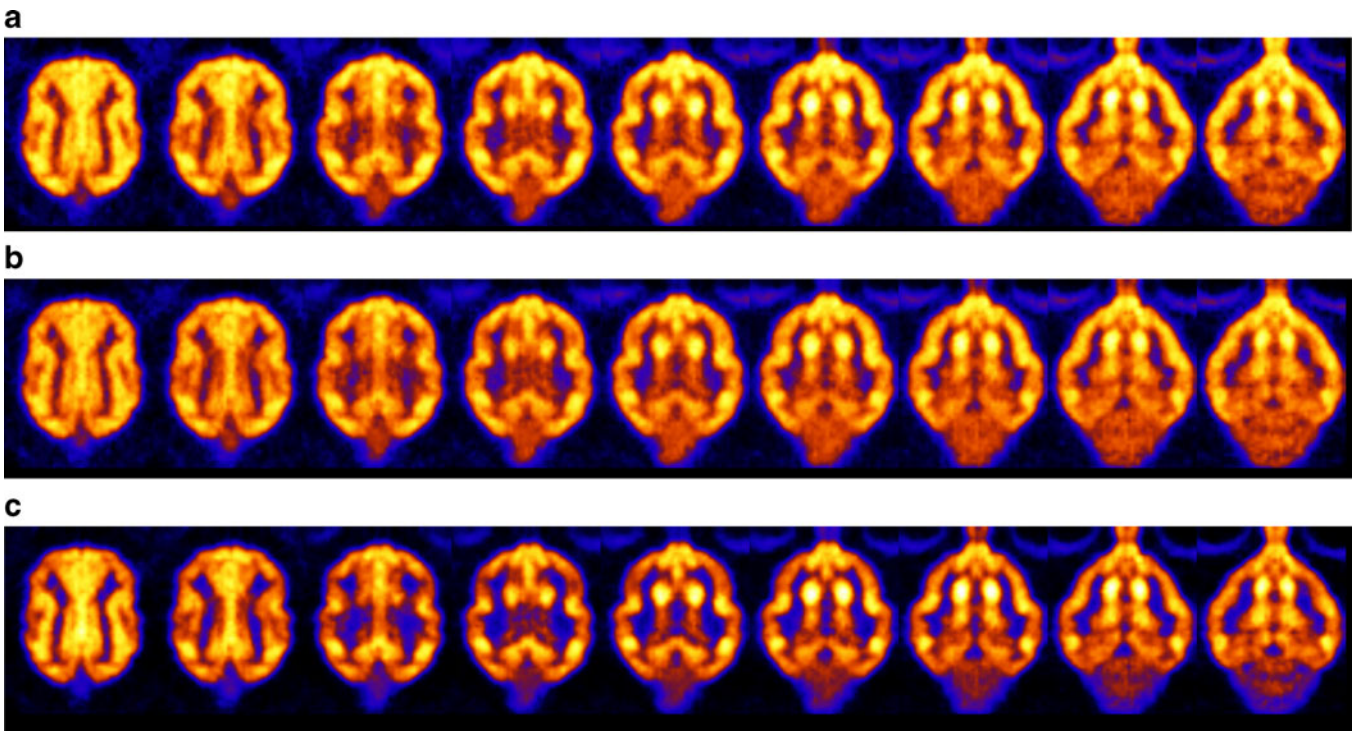

Fig. 4. Transverse images of attenuation and scatter corrected emission PET images using **a** MAC, **b** TGAC, and **c** CAC.

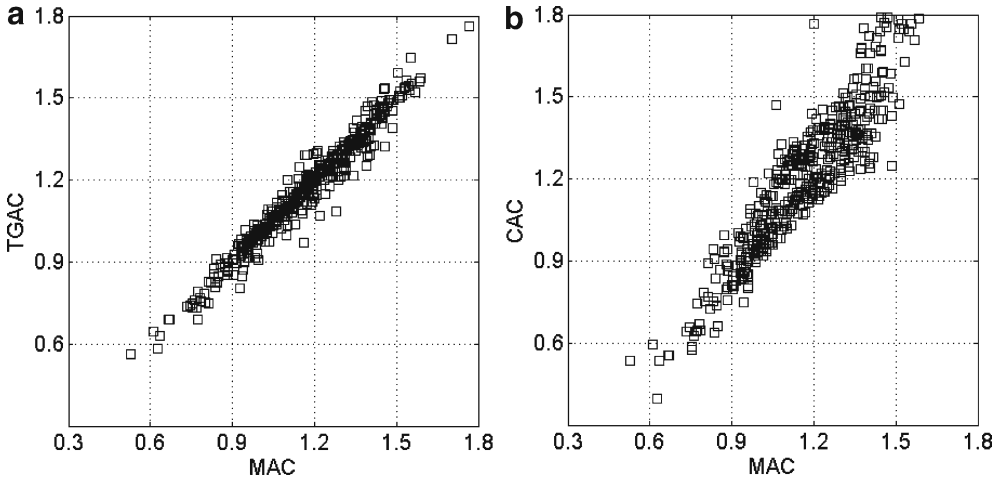

Fig. 5. Correlation plots of regional emission counts. **a** TGAC versus MAC ($y = 0.98x + 0.01$, R^2=0.96). **b** CAC versus MAC (y=x, R^2=0.84).

differentiated and the bony regions, such as the skull, were well identified in the μ-map template.

The μ-maps and ACFs generated using the MAC and TGAC are compared in Fig. 2. The findings demonstrate that the TGAC provided equivalent distribution of the attenuation coefficient and correction factor compared to the MAC. However, there was much less statistical fluctuation in intensity with the TGAC compared to the MAC. In Fig. 2c, the transverse count profiles across the middle of the μ-maps are shown to demonstrate the difference in the three different AC methodologies. The TGAC had a similar profile compared to the MAC. However, the CAC did not reflect the non-uniform distribution of the attenuation coefficient across the brain and skull regions as expected. When the percent difference between the profiles were calculated using the following equation, it was less than 10% when compared between the TGAC and MAC but higher than 25% in the skull region when compared between the CAC and MAC.

$$\%difference = \frac{|MAC - X|}{(MAC + X)/2} \times 100\ (\%),$$

where X represent TGAC or CAC.

Figure 3 shows the results of voxel-wise comparisons between the μ-maps. There were no differences between the TGAC and MAC (false detection rate corrected P<0.05, k>50). However, the CAC showed significantly lower attenuation coefficients than the MAC around the skull (blue color in Fig. 3b) and was higher in the air cavity regions such as the esophagus (red color in Fig. 3b) when the same threshold for statistical significance was applied. This was likely due to the assignment of a theoretical attenuation coefficient of soft tissue at 511 keV (0.095 cm^{-1}) to the whole head region in the CAC.

EM_{AC} images of a representative case obtained using the three different AC methodologies are shown in Fig. 4. The results show that there was almost no difference between the TGAC (middle row) and the MAC (upper row). However, a relatively low count was observed in the cerebellum with the CAC (lower row). Figure 5 shows the correlation between the regional activities obtained using the ROIs drawn on the EM_{AC} images corrected by the TX-less (y-axis) and MAC (x-axis) methods. TGAC showed a strong correlation (R^2=0.96) with MAC, and the regression line between them had almost a unit slope and no bias ($y = 0.98\,x + 0.01$; Fig. 5a). By contrast, the pairs of CAC and MAC data showed a much more scattered distribution from the regression line as shown in Fig. 5b (R^2=0.84). The

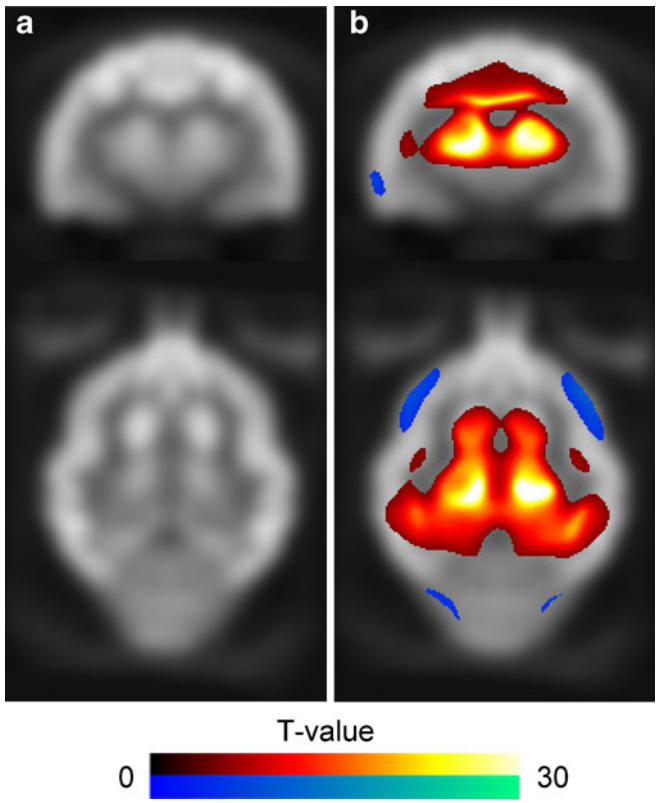

Fig. 6. The regions showing higher (*red color*) and lower (*blue color*) FDG uptake in the TGAC (**a**) and the CAC (**b**) compared to the MAC.

ROI correlation of CAC and MAC was significantly worse than that of TGAC and MAC ($P<0.05$) when they were compared using Fisher's r to Z transformation.

Voxel-wise comparisons between the EM_{AC} images corrected by the three different AC methodologies showed a similar trend as shown in the ROI analysis (Fig. 6). There were no regions with significant differences (corrected $P<0.05$, $k>50$) between the TGAC and MAC except for a small area in the cingulate cortex (MAC showed higher uptake than TGAC, Z score=5.63). However, the regional FDG uptake for the CAC was significantly higher compared to the MAC in the deep gray matter regions including the caudate and thalamus, with the same significance threshold. The FDG uptake in the neocortical regions was, by contrast, lower with the CAC than with the TGAC.

Fig. 7a shows the differences between the data sets acquired before and 4 months after the induction of deafness (group comparison). The TGAC showed results compatible with the MAC. The regional FDG uptake in the deaf state was lower than in the normal state in several regions including the temporal cortex and the inferior and superior colliculus. However, the differences in the inferior and superior colliculus could not be detected by the CAC data.

Figure 7b shows that the CAC results were opposite to the MAC results in some region (hypo- versus hyper-metabolism in frontal lobe) for the 9-month follow-up data. In the individual analysis of the deaf cats (comparison of one deaf versus eight normal), the TGAC had almost identical results with the MAC, but there was some discrepancy between the results from the CAC compared to the MAC (Table 1, Fig. 8).

Discussion

Since anesthesia can influence the global and/or regional distribution of radiotracers by interactions with biochemical pathways [27–29], PET studies on conscious animals are ideal for the accurate assessment of functional and biochemical processes in living animals. Although a specially designed PET scanner [30] or continuous motion tracking method with a slight amount of movement restriction [31] have been suggested for the PET scans of unanesthetized animals, they have not been practical for use to date. Therefore, the proper choice of the methods used as well as the minimal use of anesthesia remains the most important issues to consider for animal PET imaging studies, and the minimization of the time for the total PET study is regarded

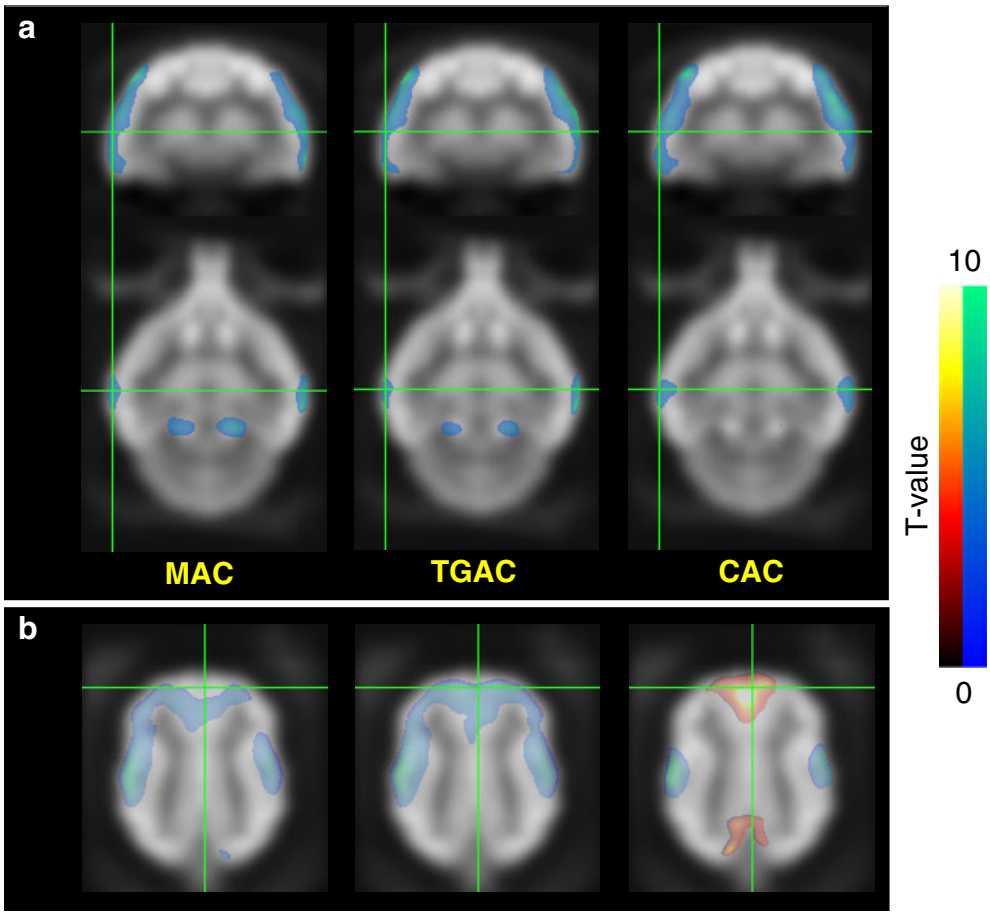

Fig. 7. The regions showing increased (*red color*) and decreased (*blue color*) FDG uptake after the induction of deafness. **a** 4 months, **b** 9 months.

Table 1. Result of individual SPM analysis (comparison of AC methods)

Cat number	Region	MAC	TGAC	CAC
1	STG	L	L/R	L/R
	MTG	L/R	R	L/R
2	STG	L/R	L/R	L/R
	MTG	L/R	L/R	L/R
3	STG	L/R	L/R	L/R
	MTG	L/R	L/R	L/R
4	STG	–	–	–
	MTG	L/R	R	R
5	STG	L/R	L/R	L/R
	MTG	L/R	L/R	R
6	STG	L/R	L/R	–
	MTG	–	–	–
7	STG	L/R	L/R	–
	MTG	L/R	L/R	–
8	STG	L/R	L/R	–
	MTG	L/R	L/R	–

L left, *R* right, *MAC* measured attenuation correction, *TGAC* template-guided attenuation correction, *CAC* calculated attenuation correction, *STG* superior temporal gyrus, *MTG* middle temporal gyrus

as one of the most important factors for use of this technology on animals.

Several methods to reduce the additional TX scanning time have been widely applied in human PET or PET/CT studies. These methods include post-EM TX scanning, simultaneous TX and EM scanning, X-ray CT-based AC, and segmented AC (SAC). However, relatively limited data are available on the use of these approaches in animal PET studies; this is mainly because of the less significant effects of attenuation and scatter of gamma rays in small animals compared to humans [1].

Post-EM TX scanning methods in small-animal PET scanners have been evaluated, and the feasibility was reported by several groups [8, 10, 13]. However, the noise due to count contamination by the EM photons in the TX data requires further correction. In a recent report [8], the count contamination by EM, in post-EM TX using a ^{57}Co source, was corrected by performing additional "mock" scanning (additional scan without external TX source for eliminating the EM count contamination) [32]. However, the necessity to perform an additional "mock" scan is a limitation of this method because the post-EM TX without "mock" scan leads to the deviation of attenuation coefficient from the theoretical value if the high emission activities exist as in the cat studies (injection dose ~110 MBq) [13].

For the integrated animal PET/CT system (i.e., Siemens Inveon and GE eXplore VISTA), a CT-based AC is a possible solution. However, most vendors do not provide this function maybe because the CT-based AC for the animal PET/CT system has not been validated completely yet. Further systematic investigation is required because of the current limitations in CT components of commercial animal PET/CT scanners, such as the beam hardening artifact that can cause the erroneous corrections of attenuation and scatter.

The SAC [14–16] is a useful technology that can be used to reduce the TX scanning time. However, there have been reports that this algorithm has limited performance for animal PET data [6, 8]. In addition, acquisition of additional TX PET scanning is a limitation of this method.

TX-less AC methods have several advantages in addition to the reduction of anesthesia use and study duration. Because the μ-map is derived from the EM data, there are no artifacts associated with subject movement between the TX and EM scans. Almost noiseless μ-maps can be obtained because the CAC assumes uniform attenuation coefficients in the same regions, and the TGAC derives the μ-map from a population data set. For repeated PET studies, for monitoring treatment efficacies in animal disease models [33–35] and investigating the functional and metabolic changes after the implementation of neural prostheses [36, 37], the TX-less AC method would be especially useful. Radiation exposure from TX scanning can be avoided, and tolerance to anesthesia due to repeated administration can be improved.

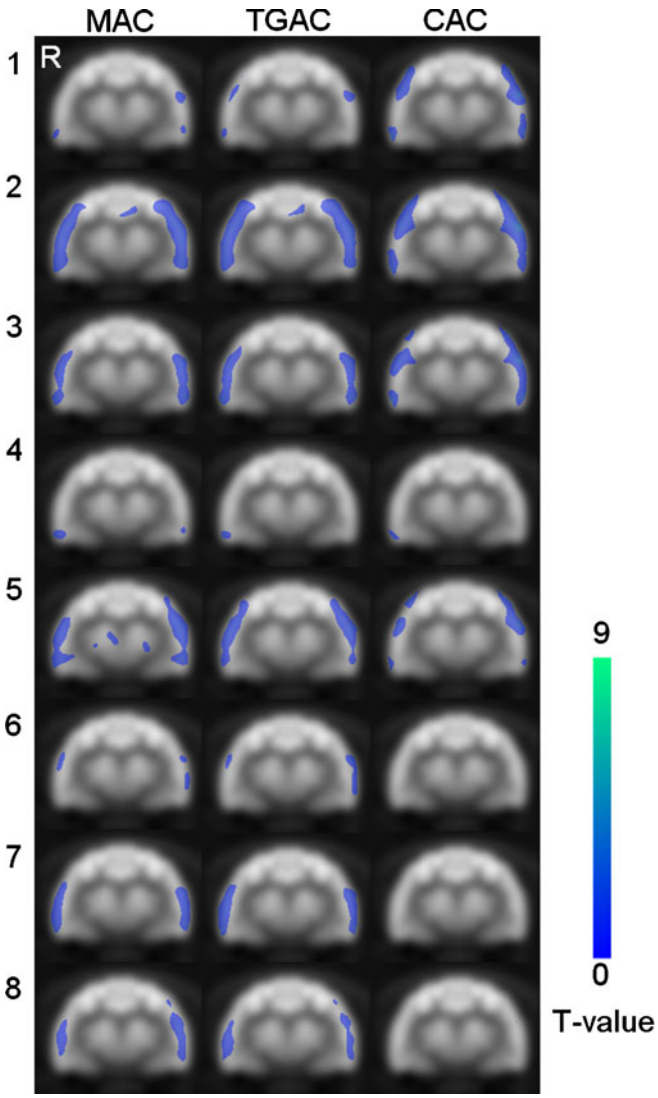

Fig. 8. Brain regions with hypometabolism in the individual analysis of the deaf cats (comparison of one deaf versus eight normal).

Integrated PET/MRI systems, based on semiconductor photo-sensors, are being actively developed [38–41]. Because performing TX scanning using rotating external radiation sources is difficult in the integrated PET/MRI systems due to insufficient space within the MRI scanner [42–44], the μ-map could be derived from either the EM PET or the MRI data. Therefore, the TX-less AC method could also be useful for the simultaneous PET/MR imaging of animals [42].

The results of the present study showed that the TGAC and MAC (the gold standard) produced almost identical intensity distributions in the μ-maps and EM_{AC}, which was validated by both the ROI and SPM analyses. In the ROI analysis, the regional distributions showed a strong correlation (R^2=0.96). For the SPM analysis, the group comparisons between normal and deaf conditions showed identical results both in the initial and follow-up studies; especially, the hypometabolism in superior and inferior colliculus and frontal lobe observed respectively in the data acquired 4 and 9 months after inducing deafness were the common findings of only the TGAC and MAC (Fig. 7). In addition, the same results were obtained for the individual assessments of reduced glucose metabolism in the auditory cortices after the induction of deafness (comparison between one deaf and eight normal cats). As shown in Table 1 and Fig. 8, the TGAC showed almost identical results with MAC except for two cats (#1 and #4). In these two cats, the statistical significance of hypometabolism in temporal lobes was relatively milder than the others. Therefore, with the given threshold of statistical significance, only the unilateral hypometabolism were observed in middle or superior temporal gyrus, depending on the AC methods. However, we could observe the common bilateral hypometabolism in these animals by the slight adjustment of the threshold, suggesting the additional evidence of the compatibility between the TGAC and MAC.

Another concern of the TGAC method was how they treat other attenuating and scatter material in the field of view, such as the bed or any supporting material for the animal. Although the bed in the scanner in the μ-maps of the MAC was seen clearer than those of TGAC (Fig. 2a and b), there were no statistical differences between MAC and TGAC in near bed region on both SPM and ROI analysis (Figs. 6 and 7). This implies that the influence of the bed of the scanner would be negligible in the TGAC method.

Because the feasibility of the TGAC has been validated only for the cat FDG brain PET, from the data collected in the present study, further investigation on the validity of this method for other radiotracers and animals is needed. The feasibility of this method for the whole body PET studies of rodents might provide an additional option for the accurate assessment of regional activity by both the semi-quantitative [35, 45] and kinetic modeling methods [46–48] used in rodents.

The CAC, another TX-less AC method tested in the present study, showed a much different pattern for the μ-map compared to the MAC; this was mainly because the attenuation coefficient was assigned uniformly across the whole head region. The lower attenuation coefficients in the bony regions, and higher attenuation coefficients in the air cavities than their actual values, led to inaccurate assessment of the regional distribution of FDG in both the cortical and subcortical regions of the brain (Fig. 6b) and different findings in the SPM group comparisons from those obtained using MAC-derived EM_{AC}. Improvement of this method is expected in a future version of the data analysis software used for microPET scanners; more sophisticated identification methods for the head contour and/or skull regions with more accurate prior knowledge of the cat anatomy will be available to improve accuracy.

Although CAC-derived μ-maps were much different from the MAC-derived data (Fig. 3b), the correlation between the regional intensities in the EM_{AC} were not as bad as expected intuitively (R^2=0.84; Fig. 5b). This is because the attenuation correction factor is not the line integration of the μ value itself but that of the $\exp(-\mu \cdot d)$, where d is the distance through the structure [49].

Conclusion

The TGAC was reliable in cat FDG brain PET studies in terms of compatibility with the MAC method. The TGAC might be a useful option for increasing study throughput and decreasing the probability of subject movement. In addition, it might reduce the possible biological effects of long-term anesthesia on the cat brain in investigations using animal-dedicated PET scanners.

Acknowledgements. This work was supported by grants from the World Class University Program (R32-10142), Atomic Energy R&D Program (2008-03852), Basic Atomic Energy Research Institute Program (M20508050002-05B0805-00210, 2008-02334), Nuclear R&D Program (M20702010002-08N0201-00200, 20090078289), and Brain Research Center of the 21st Century Frontier Research Program (M103KV010014-04K2201-01400) through the Korea Science and Engineering Foundation funded by the Ministry of Education, Science and Technology.

References

1. Pomper MG, Lee JS (2005) Small animal imaging in drug development. Curr Pharm Des 11:3247–3272
2. Riemann B, Schafers KP, Schober O et al (2008) Small animal PET in preclinical studies: opportunities and challenges. Q J Nucl Med Mol Imaging 52:215–221
3. Kalter SS, Heberling RL, Cooke AW et al (1997) Viral infections of nonhuman primates. Lab Anim Sci 47:461–467
4. Kim JS, Lee JS, Park MH et al (2008) Assessment of cerebral glucose metabolism in cat deafness model: strategies for improving the voxel-based statistical analysis for animal PET studies. Mol Imaging Biol 10:154–161
5. Knoess C, Siegel S, Smith A et al (2003) Performance evaluation of the microPET R4 PET scanner for rodents. Eur J Nucl Med Mol Imaging 30:737–747
6. Kim JS, Lee JS, Lee JJ et al (2006) Effects of attenuation and scatter corrections in cat brain PET images using microPET R4 scanner. Nucl Med Mol Imaging 40:40–47
7. Kim JS, Lee JS, Park M-H et al (2007) Limited performance of calculated attenuation correction for brain PET of cat [abstract]. J Nucl Med 48(suppl):411

8. Vandervoort E, Sossi V (2008) Impact of contamination from scattered photons in singles-mode transmission data on quantitative small-animal PET Imaging. J Nucl Med. 49:1852–1861
9. Carson RE, Daube-Witherspoon ME, Green MV (1988) A method for postinjection PET transmission measurements with a rotating source. J Nucl Med 29:1558–1567
10. Chow PL, Rannou FR, Chatziioannou AF (2005) Attenuation correction for small animal PET tomographs. Phys Med Biol 50:1837–1850
11. Burger C, Goerres G, Schoenes S, Buck A, Lonn AH, Von Schulthess GK (2002) PET attenuation coefficients from CT images: experimental evaluation of the transformation of CT into PET 511-keV attenuation coefficients. Eur J Nucl Med Mol Imaging 29:922–927
12. Kinahan PE, Townsend DW, Beyer T, Sashin D (1998) Attenuation correction for a combined 3D PET/CT scanner. Med Phys 25:2046–2053
13. Lehnert W, Meikle SR, Siegel S, Newport D, Banati RB, Rosenfeld AB (2006) Evaluation of transmission methodology and attenuation correction for the microPET Focus 220 animal scanner. Phys Med Biol 51:4003–4016
14. Nuyts J, Dupont P, Stroobants S, Benninck R, Mortelmans L, Suetens P (1999) Simultaneous maximum a posteriori reconstruction of attenuation and activity distributions from emission sinograms. IEEE T Med Imaging 18:393–403
15. Xu EZ, Mullani NA, Gould KL, Anderson WL (1991) A segmented attenuation correction for PET. J Nucl Med 32:161–165
16. Nuyts J, Dupont P, Stroobants S, Maes A, Mortelmans L, Suetens P (1999) Evaluation of maximum-likelihood based attenuation correction in positron emission tomography. IEEE T Nucl Sci 46:1136–1141
17. Stodilka RZ, Kemp BJ, Prato FS, Kertesz A, Kuhl D, Nicholson RL (2000) Scatter and attenuation correction for brain SPECT using attenuation distributions inferred from a head atlas. J Nucl Med 41:1569–1578
18. Montandon ML, Zaidi H (2005) Atlas-guided non-uniform attenuation correction in cerebral 3D PET imaging. Neuroimage 25:278–286
19. Siegel S, Dahlbom M (1992) Implementation and evaluation of a calculated attenuation correction for PET. IEEE T Nucl Sci 39:1117–1121
20. Weinzapfel BT, Hutchins GD (2001) Automated PET attenuation correction model for functional brain imaging. J Nucl Med 42:483–491
21. Kim JS, Lee JS, Im KC et al (2007) Performance measurement of the microPET focus 120 scanner. J Nucl Med 48:1527–1535
22. Rogers JG, Harrop R, Kinahan PE (1987) The theory of three-dimensional image reconstruction for PET. IEEE T Med Imaging 6:239–243
23. Huber JS, Moses WW, Jones WF, Watson CC (2002) Effect of ^{176}Lu background on singles transmission for LSO-based PET cameras. Phys Med Biol 47:3535–3541
24. Watson CC. New, faster, image-based scatter correction for 3D PET (2000) IEEE T Nucl Sci 47:1587–1594.
25. Ashburner J, Friston KJ (1999) Nonlinear spatial normalization using basis functions. Hum Brain Mapp 7:254–266
26. Friston KJ, Ashburner J, Frith CD, Poline JB, Heather JD, Frackowiak RSJ (1995) Spatial registration and normalization of images. Hum Brain Mapp 3:165–189
27. Matsumura A, Mizokawa S, Tanaka M et al (2003) Assessment of microPET performance in analyzing the rat brain under different types of anesthesia: comparison between quantitative data obtained with microPET and *ex vivo* autoradiography. Neuroimage 20:2040–2050
28. Toyama H, Ichise M, Liow JS et al (2004) Evaluation of anesthesia effects on ^{18}F-FDG uptake in mouse brain and heart using small animal PET. Nucl Med Biol 31:251–256
29. Woo SK, Lee TS, Kim KM et al (2008) Anesthesia condition for ^{18}F-FDG imaging of lung metastasis tumors using small animal PET. Nucl Med Biol. 35:143–150
30. Woody C, Kriplani A, O'Connor P et al (2004) RatCAP: a small, head-mounted PET tomograph for imaging the brain of an awake rat. Nucl Instrum Meth A 527:166–170
31. Zhou VW, Kyme AZ, Meikle SR, Fulton R (2008) An event-driven motion correction method for neurological PET studies of awake laboratory animals. Mol Imaging Biol 10:315–324
32. Smith RJ, Karp JS, Muehllehner G (1994) Post injection transmission scanning in a volume imaging PET camera. IEEE T Nucl Sci 41:1526–1531
33. Yang H, Berger F, Tran C, Gambhir SS, Sawyers CL (2003) MicroPET imaging of prostate cancer in LNCAP-SR39TK-GFP mouse xenografts. Prostate 55:39–47
34. Zhang Y, Saylor M, Wen S et al (2006) Longitudinally quantitative 2-deoxy-2-^{18}F-fluoro-D-glucose micro positron emission tomography imaging for efficacy of new anticancer drugs: a case study with bortezomib in prostate cancer murine model. Mol Imaging Biol 8:300–308
35. Lee JS, Orita H, Gabrielson K et al (2007) FDG-PET for pharmacodynamic assessment of the fatty acid synthase inhibitor C75 in an experimental model of lung cancer. Pharm Res 24:1202–1207
36. Ahn SH, Oh SH, Lee JS et al (2004) Changes of 2-deoxyglucose uptake in the rat auditory pathway after bilateral ablation of the cochlea. Hear Res 196:33–38
37. Lee JS, Ahn SH, Lee DS et al (2005) Voxel-based statistical analysis of cerebral glucose metabolism in the rat cortical deafness model by 3D reconstruction of brain from autoradiographic images. Eur J Nucl Med Mol Imaging 32:696–701
38. Judenhofer MS, Catana C, Swann BK et al (2007) PET/MR images acquired with a compact MR-compatible PET detector in a 7-T magnet. Radiology 244:807–814
39. Judenhofer MS, Wehrl HF, Newport DF et al (2008) Simultaneous PET-MRI: a new approach for functional and morphological imaging. Nat Med 14:459–465
40. Catana C, Procissi D, Wu Y et al (2008) Simultaneous *in vivo* positron emission tomography and magnetic resonance imaging. Proc Natl Acad Sci U S A 105:3705–3710
41. Hong SG, Song IC, Ito M et al (2008) An investigation into the use of geiger-mode solid-state photomultipliers for simultaneous PET and MRI acquisition. IEEE T Nucl Sci 55:882–888
42. Hofmann M, Steinke F, Scheel V et al (2008) MRI-based attenuation correction for PET/MRI: a novel approach combining pattern recognition and atlas registration. J Nucl Med 49:1875–1883
43. Kim JS, Lee JS, Cheon GJ (2008) Physical artifact correction in nuclear medicine imaging: normalization and attenuation correction. Nucl Med Mol Imaging 42:112–117
44. Beyer T, Weigert M, Quick HH et al (2008) MR-based attenuation correction for torso-PET/MR imaging: pitfalls in mapping MR to CT data. Eur J Nucl Med Mol Imaging 35:1142–1146
45. Waldherr C, Mellinghoff IK, Tran C et al (2005) Monitoring antiproliferative responses to kinase inhibitor therapy in mice with 3′-deoxy-3′-^{18}F-fluorothymidine PET. J Nucl Med 46:114–120
46. Green LA, Nguyen K, Berenji B et al (2004) A tracer kinetic model for ^{18}F-FHBG for quantitating herpes simplex virus type 1 thymidine kinase reporter gene expression in living animals using PET. J Nucl Med 45:1560–1570
47. Herrero P, Kim J, Sharp TL et al (2006) Assessment of myocardial blood flow using ^{15}O-water and 1-^{11}C-acetate in rats with small-animal PET. J Nucl Med 47:477–485
48. Kim SJ, Lee JS, Im KC et al (2008) Kinetic modeling of 3′-Deoxy-3′-^{18}F-Fluorothymidine for quantitative cell proliferation imaging in subcutaneous tumor models in mice. J Nucl Med 49:2057–2066
49. van Velden FH, Kloet RW, van Berckel BN et al (2008) Impact of attenuation correction strategies on the quantification of high resolution research tomograph PET studies. Phys Med Biol 53:99–118